J. Fluid Mech. (1992), *vol.* 243, *pp.* 653–677
Printed in Great Britain

An asymptotic theory for the linear stability of a core–annular flow in the thin annular limit

By E. GEORGIOU[1], C. MALDARELLI[1], D. T. PAPAGEORGIOU[2] AND D. S. RUMSCHITZKI[1]†

[1] Levich Institute and Chemical Engineering Department, City College of New York, New York, NY 10031, USA

[2] Department of Mathematics, New Jersey Institute of Technology, Newark, NJ 07102, USA

(Received 17 June 1991 and in revised form 27 March 1992)

We study the linear stability of a vertical, perfectly concentric, core–annular flow in the limit in which the gap is much thinner than the core radius. The analysis includes the effects of viscosity and density stratification, interfacial tension, gravity and pressure-driven forcing. In the limit of small annular thicknesses, several terms of the expression for the growth rate are found in order to identify and characterize the competing effects of the various physical mechanisms present. For the sets of parameters describing physical situations they allow immediate determination of which mechanisms dominate the stability. Comparisons between the asymptotic formula and available full numerical computations show excellent agreement for non-dimensional ratio of undisturbed annular thickness to core radius as large as 0.2.

The expansion leads to new linear stability results (an expression for the growth rate in powers of the capillary number to the $\frac{1}{3}$ power) for wetting layers in low-capillary-number liquid–liquid displacements. The expression includes both capillarity and viscosity stratification and agrees well with the experimental results of Aul & Olbrich (1990).

Finally, we derive Kuramoto–Sivashinsky-type integro-differential equation for the later nonlinear stages of the interfacial dynamics, and discuss their solutions.

1. Introduction

To recover oil which is saturating capillary pores in a rock bed one can flush with a second, immiscible liquid, usually an aqueous solution of low interfacial tension with the oil. The type of flow pattern which develops as the aqueous phase displaces the saturating oil depends on the wetting properties of the oil and the aqueous solution. If the oil wets the pore wall more strongly than the aqueous phase, then the displacement takes the form of a winding train of long aqueous slugs separated by pools of oil and riding over a thin cushion of the oil. Alternatively, if the aqueous solution is more strongly wetting, then the fluids change places, and the displacement consists of slugs of oil moving over an aqueous film. In either case, the hydraulic resistance of rock pores is usually large enough that the train velocities are small, and the flow capillary numbers $\mathbb{C}$ (defined as the product of the slug velocity U and the wetting layer viscosity divided by the interfacial tension) are usually much less than one. In addition, Reynolds numbers (defined as the product of the train velocity multiplied by the pore radius and divided by either the kinematic viscosity of the oil or the displacing phase) are commonly of order one or less. For these cases of small

† To whom correspondence should be addressed.

$\mathbb{C}$ and order-one or less Reynolds numbers, the thickness of the wetting layer is set by the conditions at the leading edge of the slug, and is proportional, from the asymptotic theory of Bretherton (1961), to $\mathbb{C}^{\frac{2}{3}}$.

In the central region of the slug, the flow locally resembles a core–annular flow (CAF) with the non-wetting phase flowing centrally, and the wetting liquid moving in an annular ring. The interfacial stability of this CAF can significantly affect the mobility of the train. Growing interfacial disturbances can cause the wetting layer to snap and bring the non-wetting fluid in contact with the capillary pore wall. If the respreading of the wetting layer is slow or inhibited, then contact line forces now attaching the slug to the wall can retard the movement of the slug and decrease the overall train mobility.

The aim of this paper is to study the linear stability of CAF in an effort to better understand the mobility of the train flows which develop in displacing oil with aqueous solutions. A first step is to examine the linear stability of a perfect core–annular flow (PCAF), which is a CAF in a vertical, precisely circular tube (radius R_2) in which the core (undisturbed radius R_1) and annulus are exactly concentric with the tube wall. Joseph and collaborators in a series of articles (Joseph, Renardy & Renardy 1984; Preziosi, Chen & Joseph 1989; Hu & Joseph 1989; Hu, Lundgren & Joseph 1990; Chen, Bai & Joseph 1990; Bai, Chen & Joseph 1992; Chen & Joseph 1991 and Chen 1992) have used numerical and long-wave techniques to establish a detailed picture of the linear stability of a PCAF mainly to axisymmetric disturbances.

Joseph and his collaborators find that when the interface separating the core and annular fluids is perturbed, the leading order (in the interfacial perturbation) capillary forces in a flowing system are identical to those in static liquid threads and annular wetting layers as studied by Plateau (1870) and Rayleigh (1879, see Chandrasekhar 1968), Tomotika (1935) and Goren (1962). They are independent of the base-state flow, and arise simply from the cylindrical geometry of the unperturbed fluid–fluid interface. In particular, the leading-order surface tension force arising from the circumferential curvature is destabilizing, while that from the axial curvature is stabilizing. For interfacial disturbances with wavelengths larger than the unperturbed core circumference, the destabilizing force dominates and these waves grow; disturbances with wavelengths less than this circumference decay.

In core–annular flows, the jump in the radial derivative of the axial base-state flow velocity generates a jump in the first-order axial velocity at the interface when the fluids are of unequal viscosity. It also leads to a jump in the first-order shear stress when the fluids are of unequal density and the flow is in a vertical tube and driven (at least partly) by gravity. The jump in axial velocity destabilizes short waves. The axial velocity jump can also destabilize long waves, but only when the annular fluid is more viscous than the core fluid; it stabilizes these waves when the annular layer is less viscous. Joseph and his co-workers demonstrate that the interplay of the effects of capillarity and the jump in axial velocity can give rise to a window of global stability: when the annulus thickness is much less than the core radius and the annular fluid is less (but not much less) viscous than the core, the long-wave stabilization due to the velocity jump stabilizes, at sufficiently large Reynolds numbers, all waves larger than the core circumference. These wavelengths would have been destabilized by capillarity. Waves shorter than the circumference are stabilized by capillarity; thus for these large Reynolds numbers, the CAF is stable to all disturbance waves. This stabilization persists to even higher values of the Reynolds number until the short-wave destabilization arising from the velocity jump

causes short waves to become unstable. This high-Reynolds-number instability exists as a band of unstable waves since the capillarity stabilizes the very shortest waves (cf. Chen 1992). When the annulus is more viscous, no such window exists; both capillarity and the axial velocity jump destabilize long waves and the axial velocity jump alone destabilizes short waves.

In vertical tubes with combined pressure and gravity forcing, as the density of the annular phase becomes larger than that of the core, the jump in tangential stress caused by the density difference stabilizes long waves when the flow is in the direction of gravity (downflow), but destabilizes them when the flow is against gravity (upflow). All of these results pertain to axisymmetric disturbances of core–annular flows; the effects of non-axisymmetric disturbances have not been systematically studied.

The objective of this study is to understand the stability of PCAF with thin layers in order to draw conclusions on the ability of wetting layers around slugs to remain intact. The studies of Joseph and co-workers outlined above cannot directly apply to the thin-layer problems considered here for several reasons. First, the layers are extremely thin; the annular thickness can be one hundredth the size of the undisturbed core radius or smaller, i.e. $\epsilon \equiv (R_2 - R_1)/R_1 = a - 1 \leqslant 10^{-2}$. Numerical calculations become extremely difficult in this limit because of the rapid variation of hydrodynamic variables in the thin wetting layer, and would require special domain stretching in order to find solutions satisfying the conditions at the ends of the layer. Indeed Joseph *et al.* have undertaken studies only down to $\epsilon = 0.1$. Also, Newhouse & Pozrikidis (1992), who use the boundary-integral technique for Stokes flow to follow an unstable wave's growth, note that calculation of the Green function requires rapidly increasing computer times as ϵ gets small. Second, our thin-film theory, as indeed any analytic theory, facilitates direct assessment of the importance of competing effects as well as the influence of the pertinent parameters. Finally, in the study of the stability of the wetting layer the computation of growth rates is essential in order to resolve how the timescale for the disturbance growth compares to the speed with which surface convection or dispersion moves the disturbance to the trailing edge of the slug; our analysis provides an easy method for generating such curves.

To avoid numerical problems, we propose studying this thin-annulus stability by constructing asymptotic solutions to the linear growth rate in the limit as $\epsilon \to 0$ with the wavenumber α and the viscosity ratio (annular to core fluid) m larger than ϵ. Since α is of order one, these asymptotic expressions describe dynamics for disturbances of the order of or larger than the core radius R_1, but not of the order of the annulus thickness. (Chen & Joseph 1991 point out that when ϵ is large or when $m = O(\epsilon)$ and ϵ is fairly small, the film's inertia becomes significant, and thus we require m to be asymptotically larger than ϵ.) In fluid–fluid displacement problems, we have remarked that Reynolds numbers $\mathbb{R}$ are of order one or smaller, and so we will take $\mathbb{R}_g$, the square root of the Reynolds number for the purely gravity-driven flow, and F, the ratio of the axial pressure gradient to the gravitational force per unit volume, to be of order one. Values of J, the dimensionless quantity that characterizes the system's surface tension, for these problems are much larger than one since $J = \mathbb{R}m/\mathbb{C}$ and the capillary number is small; we therefore take $J = O(1/\epsilon)$. Other smaller scalings for J are also considered and we will show that they can be derived from the $J = O(1/\epsilon)$ general expressions obtained by taking appropriate limits. Importantly, these other regimes are relevant to other CAF regimes such as lubricated pipelining where J is of order one or smaller in ϵ.

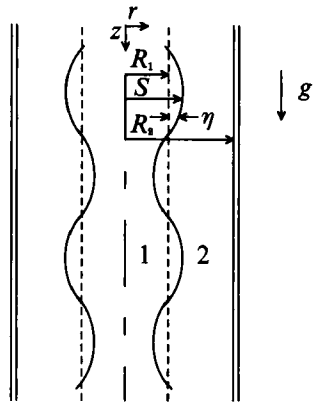

FIGURE 1. Schematic of the circular tube geometry arranged vertically.

Once derived, we use the growth rate expansion in ϵ for the following purposes. First we show that the expansion, when used to construct neutral curves, can reproduce with exceptional accuracy the lower (order-one) branches of the ($\mathbb{R}_g$ *vs.* α) and (F *vs.* α) plots obtained numerically by Joseph *et al.* for ϵ as high as 0.2. Second, we construct neutral curves for the case of $m > 1$ and we detail growth rates for both $m > 1$ and $m < 1$. Third, using the Bretherton analysis in conjunction with our asymptotic expansion, we develop a theory for the stability of the wetting layer surrounding liquid slugs moving at low capillary numbers and show that it predicts the results of Aul & Olbricht's (1990) experiments on liquid–liquid displacements in capillary tubes. We conclude with a brief description of how the expansion can be incorporated into a weakly nonlinear theory of the interface's stability.

We should note that PCAFs occur in straight channels with unchanging cross-sections, and our application of the results of PCAF stability theory to the stability of wetting layers in slug flows in porous media ignores the tortousity and constrictions of the pore channels of real rock strata. The presence of constrictions enhances the destabilizing effect of capillarity because the circumferential curvature is smaller, and the surface-tension force arising from this curvature is correspondingly larger. Gaugliz & Radke (1990) and Ratolowski & Change (1989) have examined this effect for the capillary growth of a thin static film deposited on the inside of a straight tube with an axisymmetric constriction. Our asymptotic analysis could include the influence of constrictions to some extent by considering a varying tube radius for which the lengthscale of the axial variation in the radius is much larger than the tube radius. As a first study, however, we restrict our attention to tubes of constant cross-section.

An outline of this study is as follows. In §2 we formulate the linear stability problem, and derive the exact governing equations in terms of non-dimensional variables. In §3 we derive the long-wave expansions for the exact problem and then for the asymptotic analysis. The long-wave expansions anticipate the orderings that we use to construct the asymptotic expansions in §4. With these orderings in mind we use scaling arguments to set up asymptotic solutions in the film and in the core which, when matched, produce the linear stability dispersion equations for the first two non-trivial orders in ϵ. In §§5, 6 and 7 we discuss results and applications as described in the previous paragraph.

2. Formulation of the exact linear stability theory

Two immiscible, Newtonian, incompressible fluids are flowing in a perfect core–annular arrangement in a vertical pipe of inner radius R_2. The interface is given by $r = R_1$. A fluid of viscosity μ_1 and density ρ_1 occupies the core region $0 \leqslant r \leqslant R_1$. A second fluid with viscosity μ_2 and density ρ_2 occupies the film region $R_1 \leqslant r \leqslant R_2$. We use cylindrical polar coordinates (r, θ, z) with the z-axis oriented in the direction of the gravitational acceleration $\boldsymbol{g}$ (see figure 1). Gravity and a uniform, constant pressure gradient $-\mathrm{d}P/\mathrm{d}z = f$ drive the flow. The velocity field is unidirectional and depends only on r. Non-dimensionalizing the velocity by the gravity scale $[\rho_1 g R_1^2/\mu_1]$ and the radial coordinate by the unperturbed core radius R_1, the base flow takes the following form:

$$\boldsymbol{v}_i = [0, 0, w_i^0(r)] \quad (i = 1, 2), \tag{2.1}$$

$$w_1^0(r) = \frac{F+1}{4}(1-r^2) + \frac{F+l}{4m}(a^2-1) + \frac{1-l}{2m}\ln a, \quad 0 \leqslant r \leqslant 1, \tag{2.2}$$

$$w_2^0(r) = \frac{F+l}{4m}(a^2-r^2) - \frac{1-l}{2m}\ln\left(\frac{r}{a}\right), \quad 1 \leqslant r \leqslant a, \tag{2.3}$$

where subscripts 1 and 2 denote the core and annular regions respectively. The non-dimensional parameters

$$F = \frac{f}{\rho_1 g}, \quad m = \frac{\mu_2}{\mu_1}, \quad l = \frac{\rho_2}{\rho_1}, \quad a = \frac{R_2}{R_1} \tag{2.4}$$

appear in (2.2) and (2.3) as a result of the non-dimensionalization proposed above. The parameter F is a measure of the effect of pressure forcing on the flow direction in a vertical tube; for $l = 1$, when $F > -1$ the flow is downward, and when $F < -1$ pressure overcompensates for gravity and the flow is upward. When l is not equal to one, these demarcations are not strictly valid and mixed flow can occur. However, assuming that the density differences are not too great, when $F < -1$ the flow is predominantly up and when $F > -1$ the flow is predominantly down, and therefore in this paper we refer loosely to these ranges of F as 'upflow' and 'downflow'.

Consider axisymmetric disturbances of the interface $r(z,t) = S(z,t)$ which cause velocity disturbances to the core and annular base flows. All equations that follow are in non-dimensional form with radial and axial variables non-dimensionalized by R_1, velocities by $[\rho_1 g R_1^2/\mu_1]$ time by $[\mu_1/(\rho_1 g R_1)]$ and pressure by $[\rho_1^3 g^2 R_1^4/\mu_1^2]$. Since the fluids are incompressible, introduction of a disturbance stream function Ψ,

$$u_i = \frac{1}{r}\frac{\partial \Psi_i}{\partial z}, \quad w_i = -\frac{1}{r}\frac{\partial \Psi_i}{\partial r}, \tag{2.5}$$

automatically satisfies the continuity equation for the velocity disturbance.

The surface and the velocity disturbances can be ordered with a small parameter δ:

$$r(z,t) = 1 + \eta(z,t)\,\delta + O(\delta^2), \tag{2.6}$$

$$\Psi_i(r) = \Psi_i^0(r) + \Psi_i^1(r)\,\delta + O(\delta^2). \tag{2.7}$$

We then insert these expansions into the Navier–Stokes equations and kinematic and stress boundary conditions at the fluid interface. Decomposition of the resulting equations into normal modes

$$\Psi_i^1(r) = \psi_i(r) \exp[\mathrm{i}\alpha(z-ct)], \tag{2.8}$$

and retention of only order-δ terms define the following linear stability problem:

$$\mathrm{D}(\mathrm{D}\psi_1) = \mathrm{i}\alpha\mathbb{R}_g^2(w_1^0 - c)\,\mathrm{D}\psi_1, \tag{2.9}$$

and

$$\mathrm{D}(\mathrm{D}\psi_2) = \mathrm{i}\alpha\mathbb{R}_g^2\frac{l}{m}\left[(w_2^0 - c)\,\mathrm{D}\psi_2 + \left(\frac{1}{r}w_{2_r}^0 - w_{2_{rr}}^0\right)\psi_2\right], \tag{2.10}$$

where

$$\mathrm{D} \equiv \frac{\mathrm{d}^2}{\mathrm{d}r^2} - \frac{1}{r}\frac{\mathrm{d}}{\mathrm{d}r} - \alpha^2,$$

subscripts r denote differentiation, α is the wavenumber, c is the wave speed and w_i^0 is the non-dimensional base velocity in region i, subject to

$$\frac{\psi_2}{r} = 0 \quad \text{and} \quad \frac{1}{r}\frac{\mathrm{d}\psi_2}{\mathrm{d}r} = 0 \quad \text{at} \quad r = a, \tag{2.11}$$

$$\frac{\psi_1}{r} < \infty \quad \text{and} \quad \frac{1}{r}\frac{\mathrm{d}\psi_1}{\mathrm{d}r} < \infty \quad \text{at} \quad r = 0, \tag{2.12}$$

$$\frac{1}{r}(\psi_1 - \psi_2) = 0 \quad \text{at} \quad r = 1, \tag{2.13}$$

$$\frac{1}{r}\left(\frac{\mathrm{d}\psi_1}{\mathrm{d}r} - \frac{\mathrm{d}\psi_2}{\mathrm{d}r}\right) - \frac{F+1}{2m}(m-1)\,\eta = 0 \quad \text{at} \quad r = 1, \tag{2.14}$$

$$[\mathrm{D}\psi_1 + 2\alpha^2\psi_1] - m[\mathrm{D}\psi_2 + 2\alpha^2\psi_2] + r(l-1)\,\eta = 0 \quad \text{at} \quad r = 1, \tag{2.15}$$

$$\frac{m}{\mathrm{i}\alpha r}\frac{\mathrm{d}}{\mathrm{d}r}[\mathrm{D}\psi_2] + 2m\alpha\mathrm{i}\frac{\mathrm{d}}{\mathrm{d}r}\left[\frac{1}{r}\psi_2\right] - \frac{1}{\mathrm{i}\alpha r}\frac{\mathrm{d}}{\mathrm{d}r}[\mathrm{D}\psi_1] - 2\alpha\mathrm{i}\frac{\mathrm{d}}{\mathrm{d}r}\left[\frac{1}{r}\psi_1\right] - \frac{J}{\mathbb{R}_g^2}[\alpha^2 - 1]\,\eta$$
$$+ \frac{\mathbb{R}_g^2}{r}\left[(w_1^0 - c)\left(\frac{\mathrm{d}\psi_1}{\mathrm{d}r} - l\frac{\mathrm{d}\psi_2}{\mathrm{d}r}\right) + (lw_{2_r}^0 - w_{1_r}^0)\,\psi_1\right] = 0 \quad \text{at} \quad r = 1, \tag{2.16}$$

and

$$\eta = \frac{1}{r}\frac{\psi_1}{(w_1^0 - c)} \quad \text{at} \quad r = 1. \tag{2.17}$$

The dimensionless parameters

$$\mathbb{R}_g = \left[\frac{g\rho_1^2 R_1^3}{\mu_1^2}\right]^{\frac{1}{2}}, \quad J = \frac{\sigma R_1 \rho_1}{\mu_1^2}, \quad J^* = Ja, \tag{2.18}$$

appear in (2.9)–(2.17) as a result of the non-dimensionalization proposed above. $\mathbb{R}_g^2$ is the Reynolds number for pure gravity-driven flow and J is a surface-tension parameter introduced by Chandrasekhar (1961) in his study of the capillary instability of jets of a viscous liquid in air. J^* is included so that all of the notation is consistent with Chen *et al.* (1990), referred to hereinafter as CBJ). For the case of density-matched fluids ($l = 1$) (Preziosi *et al.* 1989), the maximum base velocity V occurs at the centreline, and the stability analysis does not depend separately on $\mathbb{R}_g$ and F, but rather on these variables through the product

$$\mathbb{R}_g^2\frac{(1+F)(m+a^2-1)}{4m}$$

which defines a core Reynolds number $\mathbb{R}$ based on the centreline velocity ($\mathbb{R} = \rho_1 R_1 V/\mu_1$).

3. Long-wave expansions

We now turn to the stability problem for the longest waves and for thin films. Our aim is to see the ϵ-dependence of the various effects and to anticipate the scalings for our more general asymptotic theory. Consider the stability problem for waves which are long with respect to the undisturbed core radius R_1. Using Yih's (1967) method, we introduce a regular expansion in α for the stream function ψ_i and the wave speed c:

$$c = c^{[0]} + c^{[1]}\alpha + O(\alpha^2), \tag{3.1}$$

and

$$\psi_i = \psi_i^{[0]} + \psi_i^{[1]}\alpha + O(\alpha^2). \tag{3.2}$$

These expansions assume ϵ to be an order-one quantity in α, and are thus *exact* long-wave expansions. Hickox (1971), Joseph and co-workers, and Smith (1989) (for the case $m = 1$) have computed $c^{[0]}$ and $c^{[1]}$ for ϵ of order one. We consider here the behaviour as $\epsilon \to 0$.

Substituting the above expansions into the governing equations and boundary conditions we find that $c^{[0]}$ is real and therefore does not contribute to the stability, but only to a dispersion that makes waves move with a velocity different from the base velocity at the interface:

$$c^{[0]} - w_1^0(1) = \frac{((1+\epsilon)^2-1)^2}{4m((1+\epsilon)^4+m-1)}(F+1)(m-1) - \frac{2((1+\epsilon)^4+m-1)\ln(1+\epsilon) - ((1+\epsilon)^2-1)(m+2(1+\epsilon)^2-2)}{4m((1+\epsilon)^4+m-1)}(l-1), \tag{3.3}$$

To the next order in α, we find $c^{[1]}$ to be pure imaginary; so it does contribute to the stability:

$$c^{[1]} = \left[\frac{J}{\mathbb{R}_g^2} f_1(\epsilon, m) + \mathbb{R}_g^2 f_2(\epsilon, m, l, F)\right] \mathrm{i}, \tag{3.4}$$

where f_1 and f_2 are lengthy algebraic expressions detailed in the appendix to CBJ.

We study the linear stability for long waves in the limit of small film thickness ($\epsilon \to 0$) by Taylor expanding (3.4) in powers of ϵ:

$$c^{[1]} = \frac{J}{\mathbb{R}_g^2}\left[\frac{\epsilon^3}{3m} - \frac{\epsilon^4}{m^2}\right]\mathrm{i} + \mathbb{R}_g^2 \frac{F+1}{4}\left[(m-1)\left(\frac{(F+1)}{48m^2}\epsilon^2 - \frac{(F+1)(m+8)}{48m^3}\epsilon^3\right) - \frac{(l-1)}{24m^2}\epsilon^3\right]\mathrm{i} + \ldots. \tag{3.5}$$

The first square-bracketed term on the right-hand side of (3.5) represents the destabilizing effect of the circumferential curvature; the stabilizing effect of the longitudinal curvature enters at a higher order in α. The second square-bracketed term represents the contributions of viscosity and density stratification. Equation (3.5) indicates that viscosity stratification has a stabilizing effect when $m < 1$ for both downflow ($F > -1$) and upflow ($F < -1$) and a destabilizing effect when $m > 1$. On the other hand, density stratification has a stabilizing effect for downflow and a destabilizing effect for upflow when $l > 1$ and the opposite when $l < 1$. From (3.5) we draw four important conclusions concerning the effects of capillarity, and viscosity and density stratifications for long waves on thin films. First, for $\mathbb{R}_g^2$ of order one in ϵ, the destabilizing effect of capillarity can only compete with the stabilizing

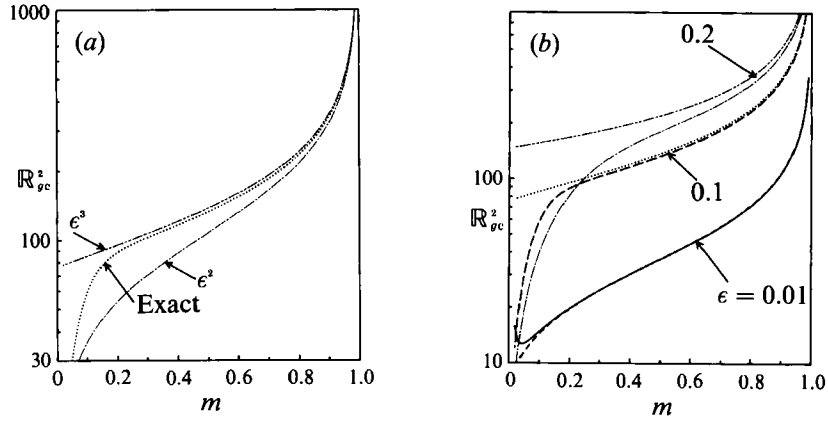

FIGURE 2. Comparison of the lubrication results with the exact solution for long waves ($\alpha \to 0$) at $J^* = 2000$. (*a*) Comparison of the order-ϵ^2 with the order-ϵ^3 solution for $\epsilon = 0.1$. (*b*) ϵ-dependence for the order-ϵ^3 solution: ——, – – –, —·—, exact; ---, ·····, ——··——, lubrication results.

effect of viscosity stratification ($m < 1$) when J is of order $1/\epsilon$. Second, the influence of density differences is one order in ϵ higher than viscosity stratification. Third, when the fluids are viscosity matched, competition between stabilizing density stratification occurs for $J = O(1)$. Lastly, we note that the expansion (3.5) is non-uniform in m as $m \to 0$. The region of non-uniformity appears to be of order ϵ because it is at this order of m that the ϵ^2 and ϵ^3 terms become comparable. Below we extend these observations for small α to a theory valid up to order one in α.

As mentioned in the introduction, neutral curves of $\mathbb{R}_g$ against α intersect the ordinate at a single point. This point derives implicitly from (3.4) by setting $c^{[1]} = 0$ and is given by

$$\mathbb{R}^4_{gc} = \frac{\mathrm{J f_1}(\epsilon, m)}{f_2(\epsilon, m, l, F)}. \tag{3.6}$$

This value is a critical Reynolds number since on the $\alpha = 0$ axis, the longest waves are stable for $\mathbb{R}_g > \mathbb{R}_{gc}$ and are unstable for $\mathbb{R}_g < \mathbb{R}_{gc}$. This region of global stability typically starts either at R_{gc} or at a value of $\mathbb{R}_g$ close to $\mathbb{R}_{gc}$.

Expanding $\mathbb{R}^4_{gc}$ in (3.6) in powers of ϵ gives us our first opportunity to evaluate how well an asymptotic expansion in ϵ reflects the exact stability picture as $\epsilon \to 0$: figure 2(*a*) compares the exact solution to (3.6) with the order-ϵ^2 and -ϵ^3 approximations to it as a function of m for $\epsilon = 0.1$, $l = 1$ and $J^* = 2000$. It is clear from figure 2(*a*) that the order-ϵ^3 expression is a significant improvement over the order-ϵ^2 expression. Figure 2(*b*) compares the agreement for different values of ϵ. It demonstrates that for fixed ϵ the agreement begins to break down for m of order ϵ; this is consistent with the fact that the region of non-uniformity in m of (3.5) is of order ϵ. As ϵ increases not only does the applicable range of m decrease, but also the accuracy of the ϵ^3 approximation decreases.

4. Asymptotic expansions

In this section we derive the asymptotic expansions in the scaled film thickness ϵ as $\epsilon \to 0$ for a Reynolds number that is order one in ϵ. The axial lengthscales in the film and in the core, and the radial lengthscale in the core remain order-one quantities while the radial lengthscale in the film is small ($O(\epsilon)$). Thus lubrication

equations will be valid in the film. In order to separate the radial lengthscales in the film and in the core, we introduce a new, order-one, stretched film variable y given by

$$r = 1 + \epsilon - \epsilon y. \tag{4.1}$$

This stretched film radial scale forces the radial derivatives in the film to be large ($O(1/\epsilon)$), whereas they are order one in the core. This will motivate a set of scalings which, as we shall see, agrees with that suggested from the long-wave analysis (cf. (3.5)) given earlier.

From the problem formulation in §2, one can see that the perturbation flows derive from the interfacial displacement η appearing in the normal and tangential stress balances and in the continuity of axial velocity boundary conditions. As such, the circumferential curvature forces ($J \neq 0$) in the normal stress balance can generate a perturbation pressure, the viscosity stratification ($m \neq 1$) can generate a large perturbative axial velocity or the density difference ($l \neq 1$) can cause a perturbative tangential stress; in principle, any one or any combination of these effects can drive the perturbation flows.

In typical, thin, lubricating film problems, it is the large perturbation pressure that sets the variables' scales. As we shall see below, this important case leads to a set of consistent scalings that are relevant to liquid–liquid displacement in rock pores. Interestingly, essentially the same scales and their resulting analysis will apply even when the surface tension is no longer as overwhelming. Thus, we shall construct an analytic structure sufficiently general to encompass all cases where F and $\mathbb{R}_g^2$ are order one or less in ϵ, J is of any order in ϵ and m is asymptotically larger than ϵ. The resulting asymptotic expressions for the growth rate c_i will be valid for any ϵ-orderings of these parameters in these ranges; insertion of a chosen set of such asymptotic orderings into c will immediately yield the dominant effects for the flow's leading-order linear stability. The long-wavelength analysis (3.5) basically foresaw this confluence of formalism for the various regimes.

Let us begin with the first case where the circumferential curvature induces a pressure perturbation across the interface that sets the fluids in motion and drives the lubrication film flow. In the stream function formalism, one uses the first-order equations of motion to represent the perturbation pressures in terms of Ψ. In the normal stress balance (2.16), the first-order derivatives are the viscous normal stresses while the third radial derivative terms and the terms multiplied by $\mathbb{R}_g^2$ are the perturbation pressures. Since radial derivatives in the film are large, the third-derivative term for the film must balance the curvature terms:

$$\frac{m}{\mathrm{i}\alpha r}\frac{1}{\epsilon^3}\frac{\mathrm{d}^3\psi_2}{\mathrm{d}y^3} = \frac{J}{\mathbb{R}_g^2}(\alpha^2 - 1)\,\eta.$$

Since α, η, m and r are all order-one quantities, the tension of the perturbation's curvature induces a film flow of order

$$\psi_2 \sim J\epsilon^3/\mathbb{R}_g^2.$$

The continuity of axial velocity at the interface (2.14) is the source of Yih's viscous stratification instability. For $m \neq 1$, the order-one term $(w_{1_r}^0 - w_{2_r}^0)\,\eta$ represents, in linearized form, the discontinuity of the base flow at the disturbed interfacial position. This introduces a perturbation to the core velocity $(1/r)(\mathrm{d}\psi_1/\mathrm{d}r)$ and possibly to the film velocity to preserve the continuity of velocity at the interface. (If the film quantity alone dominated in (2.14) it would also dominate in (2.15) and

overdetermine the film.) Let us first consider the case where the core alone takes up this perturbation. Noting that core radial derivatives are order-one quantities gives $\psi_1 \sim 1$. As a result both the leading-order continuity of radial (2.13) and axial (2.14) velocity equations involve only core quantities, while the leading-order normal stress balance is purely a film equation. These velocity conditions state that from the perspective of the leading-order core problem, the film is radially immobile, and the core alone must compensate for the perturbation-generated axial velocity jump.

In order not to overdetermine the core, the tangential stress balance must contain the dominant film term

$$\frac{m}{\epsilon^2}\frac{\mathrm{d}^2\psi_2}{\mathrm{d}y^2}$$

at leading order. Thus,

$$J\epsilon/\mathbb{R}_g^2 \geqslant \psi_1 \sim 1.$$

Equality in this expression couples the film and core through this boundary condition whereas strict inequality would require a surface tension so strong that the film alone could accommodate both the shear stress and normal stress perturbation; the film problem would close independently of the core, thereby leading to Plateau's instability for $\alpha \gtrless 1$, i.e. linear growth totally governed by capillarity with

$$J/\mathbb{R}_g^2 \sim 1/\epsilon^{1+\delta} \quad (0 \leqslant \delta < 1).$$

(An even stronger surface tension $J/\mathbb{R}_g^2 \geqslant 1/\epsilon^2$ would naturally also close the film problem and lead to Plateau's instability. It would, however, cause the film to take up some ($=$) or all ($>$) of the axial velocity perturbation and raise ($>$) the order of Ψ_1 in ϵ.) In the case of interest here, a strong yet less overwhelming surface tension (i.e. both core and film in the tangential stress balance)

$$J\epsilon/\mathbb{R}_g^2 \sim \psi_1 \sim 1$$

requires the core to find a radially immobile film, i.e. the perturbation core velocity takes up the total axial velocity discontinuity to leading order. Finally, the kinematic condition written in a frame moving with the base-flow velocity at the unperturbed interface in terms of film variables yields $(c - w^0(1)) \sim \psi_2$. Thus the complete set of scales is

$$J/\mathbb{R}_g^2 \sim \frac{1}{\epsilon}, \quad \psi_1 \sim 1, \quad \psi_2 \sim J\epsilon^3/\mathbb{R}_g^2 \sim \epsilon^2, \quad c - w^0(1) \sim \epsilon^2. \tag{4.2}$$

Let us turn now to the opposite case where the surface tension parameter J is smaller, say $J \leqslant O(1)$ in ϵ, as is the case for lubricated pipelining. J, now of reduced importance, no longer determines the scales. In fact, the third-derivative term for the film dominates the normal stress balance (2.16) and is thus zero at the interface:

$$-\frac{2mi\alpha}{r\epsilon^3}\frac{\mathrm{d}^3\psi_2}{\mathrm{d}y^3} = 0 \quad \text{at} \quad r = 1.$$

This has at least four pertinent consequences: (i) the perturbation pressure across the interface is now zero to leading order; thus, (ii) the leading-order velocity profile of the film is linear rather than parabolic; and (iii) the scale on ψ_2 must be

$$\psi_2 > O(J\epsilon^3/\mathbb{R}_g^2), \quad \text{i.e.} \quad J/\mathbb{R}_g^2 < O(\psi_2/\epsilon^3);$$

and (iv) the leading-order normal stress boundary condition again involves only film quantities.

From the long-wave analysis, one sees that, when $m \neq 1$, viscosity stratification is more important than density stratification, and is therefore the only perturbation to drive the flow. In order for the film problem neither to be overdetermined nor to have a trivial solution, the core again takes up the axial velocity perturbation and requires $\psi_1 \sim 1$. The $O(1)$ core flow only exerts an $O(1)$ tangential stress on the annulus which only drives an $O(\epsilon)$ axial flow there. Thus (and to avoid overdetermining the core) the tangential stress balance must again contain both film and core contributions, which finally requires $\psi_2 \sim \epsilon^2$ and $c - w^0(1) \sim \epsilon^2$. From the normal stress balance $(J/\mathbb{R}_g^2) < O(1/\epsilon)$, which for $\mathbb{R}_g^2 = O(1)$ allows J to be of order one or less, as in lubricated pipelining. Viscosity stratification alone (cf. (3.5)) determines the thin-film leading-order linear stability according to the sign of $m-1$; the density difference provides an order-ϵ correction.

Finally, a third set of scales that suppresses viscous stratification ($m = 1$), shows that the density difference drives an interfacial shear which can interact with a weak capillarity at leading order. By similar arguments, η causes a perturbation shear stress in both phases leading to $\Psi_1 = O(1)$, $\Psi_2 = O(\epsilon^2)$, order-one core flows and $O(\epsilon)$ axial and $O(\epsilon^2)$ radial film flows.

All three arguments above lead to the same derived scales for the dependent variables:

$$c - w^0(1) = \bar{c}^{(2)}\epsilon^2 + \bar{c}^{(3)}\epsilon^3 + \ldots, \tag{4.3}$$

$$\psi_2 = \psi_2^{(2)}\epsilon^2 + \psi_2^{(3)}\epsilon^3 + \ldots, \tag{4.4}$$

$$\psi_1 = \psi_1^{(0)} + \psi_1^{(1)}\epsilon + \ldots, \tag{4.5}$$

and $\eta = O(1)$. A single, unified treatment will use (4.3)–(4.5) in (2.9)–(2.17) to assemble the leading-order problem whose solutions are expressions for the wave speed and the growth rates. As noted, the core dynamics will couple non-trivially to those of the film through the mechanisms of viscosity stratification and density difference; this will necessitate solution of both the film and the core problems and their matching at the interface.

The derivation of the amplitude equation in terms of the wave speed c using these expansions is outlined in the Appendix and the result is

$$\bar{c}^{(2)} = -\frac{J_0}{3m\mathbb{R}_g^2}\alpha(\alpha^2-1)\,\mathrm{i} + \frac{1}{m}\frac{F+1}{4}\left[-\frac{N(\alpha)}{\alpha}\left(1-\frac{1}{m}\right)\right] + \frac{(l-1)}{2m}, \tag{4.6}$$

$$\bar{c}^{(3)} = -\frac{J_0 N(\alpha)}{\mathbb{R}_g^2 4m^2}(\alpha^2-1)\,\mathrm{i} + \left[-\frac{1}{6m} + \frac{N(\alpha)}{2\alpha m^2}\right](l-1) - \left[\frac{2\alpha^2}{3m} + \frac{2T(\alpha)-N(\alpha)}{6\alpha m} + \frac{N^2(\alpha)}{2\alpha^2 m^2}\right]\left(1-\frac{1}{m}\right)\frac{F+1}{2}, \tag{4.7}$$

where $J_0 = J\epsilon$ and $N(\alpha)$ and $T(\alpha)$, detailed in the Appendix, are in general complex. From (4.6) and (4.7) one can immediately conclude that in the strong-surface-tension case [$J = O(1/\epsilon)$], the density difference only contributes to dispersion to leading order in ϵ.

Comparison with the long-wave expansion in the previous section suggests that the combination of these results for two orders of ϵ will give excellent agreement with the exact results. It is interesting to note that in the long-wave limit ($\alpha \to 0$) (4.6) and (4.7) reduced to (3.5) by asymptotically taking the limit of $N(\alpha)$ and $T(\alpha)$ as ($\alpha \to 0$):

$$\lim_{\alpha \to 0} N(\alpha) = -4\alpha - \frac{\mathbb{R}_g^2(F+1)\alpha^2}{48}\mathrm{i},$$

and $$\lim_{\alpha \to 0} T(\alpha) = -4\alpha + \frac{\mathbb{R}_g^2 (F+1)\alpha^2}{48} \mathrm{i}.$$

It is also important to note that if the flow becomes asymptotically slow, i.e. $\mathbb{R}_g^2 = O(\epsilon)$ the complex Kummer functions reduce to real-valued modified Bessel functions. Thus, to this order, viscosity and density stratifications contribute only dispersion in this limit. In fact, this is also true for the exact problem (i.e. even for thick films) for asymptotically small values of $\mathbb{R}_g^2$.

The main task in the numerical calculation based on (4.6) and (4.7) that appears below is the accurate evaluation of the kernels $N(\alpha)$ and $T(\alpha)$ for each value of α. For moderate values of α we use an NCAR Bessel function package to calculate the Bessel functions. The calculation of the Kummer function $M(\Lambda, 2, 2\lambda r^2)$ is more complicated, however. Following Papageorgiou, Maldarelli & Rumschitzki (1990) we obtain the Kummer function for each α by numerical integration of the ordinary differential equation (A 1) (in terms of $g(r)$ where $\mathrm{D}\psi_1^{(0)} = g(r)$) in the complex plane along a contour joining 0 to 2λ. For convenience we use a straight line contour and store the values of M at the mesh points in order to compute $N_1(\alpha)$ and $N_2(\alpha)$ by quadrature from (A 19) and (A 20). A fourth-order Runge–Kutta method is used to perform the integration of the differential equation and Simpson's rule for the quadrature. Refinement tests are made to ensure numerical convergence. The extension to negative values of α follows from the identity

$$N(-\alpha) = -N^*(\alpha), \tag{4.8}$$

where * denotes complex conjugate. When a contour from 0 to $2\lambda^*$ is used in the computation of a Kummer function in the complex plane (as in the case of upflow ($F < -1$)), the result is $N^*(\alpha)$. With the kernels known numerically, the numerical implementation is now complete.

5. Results and discussion

5.1. *Neutral curves*

We begin with a discussion of neutral curves. Neutral conditions follow by equating the imaginary part of c to zero. This leads to an implicit dependence of $\mathbb{R}_g^2$ or F on the critical wavenumber α which may be expanded in ϵ:

$$\mathbb{R}_g^2 = \mathbb{R}_g^{2(0)} + \mathbb{R}_g^{2(1)}\epsilon + \ldots, \tag{5.1}$$

$$F = F^{(0)} + F^{(1)}\epsilon + \ldots. \tag{5.2}$$

Inserting either of these expressions into the defining relation for the neutral state,

$$\mathrm{Im}\,[c(\mathbb{R}_g^2, F, \epsilon, J, m, \alpha)] = 0,$$

and noting the expansion for c, leads to equations for the expansion coefficients in (5.1) and (5.2). For example, in terms of the Reynolds number:

$$\bar{c}_\mathrm{i}^{(2)}[\mathbb{R}_g^{2(0)}] = 0, \tag{5.3}$$

$$\mathbb{R}_g^{2(1)} \frac{\mathrm{d}\bar{c}_\mathrm{i}^{(2)}}{\mathrm{d}\mathbb{R}_g^2}\bigg|_{\mathbb{R}_g^{2(0)}} + \bar{c}_\mathrm{i}^{(3)}(\mathbb{R}_g^{2(0)}) = 0. \tag{5.4}$$

Newton–Raphson-based schemes provide numerical solutions for $\mathbb{R}_g^{2(0)}$ from (5.3); $\mathbb{R}_g^{2(1)}$ is obtained by evaluating the derivative in (5.4) numerically. The determination

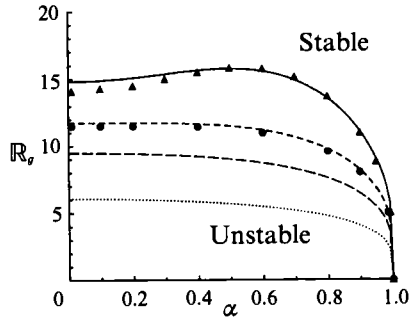

FIGURE 3. The ϵ-dependence of the free-fall flow neutral curves ($\mathbb{R}_g$ *vs.* α) ($\epsilon = 0.2$ (——), 0.1 (----), 0.05 (– – –), 0.01 (·····)) and comparison with CBJ (▲, ●). $l = 1$, $m = 0.5$, $J^* = 2000$.

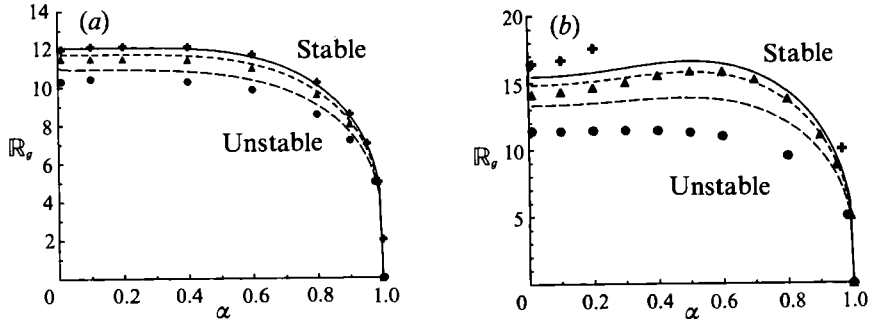

FIGURE 4. The l-dependence of the free-fall flow neutral curves [$\mathbb{R}_g$ *vs.* α] for $m = 0.5$, $J^* = 2000$ ($l = 0.5$ (——), 1.0 (---), 2.0 (— — —)) and comparison with CBJ ($l = 0.5$ (+), 1.0 (▲), 2.0 (●)). (*a*) $\epsilon = 0.1$, (*b*) $\epsilon = 0.2$.

of further terms in (5.1) and (5.2) requires expanding c to higher order. However, we show below that the two-term expansion is usually sufficient for $\epsilon < 0.2$ when $m > O(\epsilon)$.

5.1.1. *The case of the less viscous annulus* ($m < 1$)

Figure 3 shows neutral curves for pure gravity-driven flow for different values of the film thickness ϵ. From this figure one can see that the agreement between our asymptotic calculations (lines) and CBJ's results (points) is excellent even for relatively large values of ϵ ($\epsilon \leqslant 0.2$). These curves demonstrate CBJ's result that viscosity stratification stabilizes the capillary instability and that this stabilization becomes more effective the thinner the film, i.e. it becomes stable at smaller values of $\mathbb{R}_g$. Figure 4(*a*, *b*) also shows $\mathbb{R}_g$ *vs.* α neutral curves but for different values of l with m, J, and F as in figure 3. As noted in the last section and evident in figure 4, the influence of $l \neq 1$ is an order-ϵ effect on the $l = 1$ neutral curve. It is apparent from the very good agreement with CBJ that this provides a sufficient description of this effect for thin films. For $\epsilon = 0.2$, $l \neq 1$, the agreement is less satisfactory. Since the effect of $l \neq 1$ on growth first enters at $O(\epsilon^3)$, it is thus only accounted for here to its leading order in ϵ. In particular, for $l = 2$, a smaller value of ϵ is needed for order-ϵ accuracy in $\mathbb{R}_g$. For $l = 0.5$, CBJ's curve is actually no longer of the canonical form displaying global stability. In fact the branch beginning from the $\mathbb{R}_g$-axis increases rapidly to high values of $\mathbb{R}_g$ beyond $\alpha \sim 0.3$ and thus lies outside the domain of our order-one $\mathbb{R}_g$ theory. Again, as CBJ note, one should use a heavier lubricant to achieve stability at lower values of $\mathbb{R}_g$ for pure gravity-driven flows.

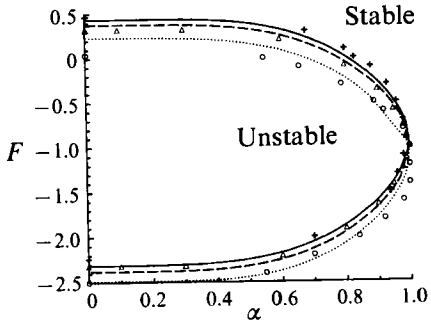

FIGURE 5. The l-dependence of the forced-flow neutral curves [F *vs.* α] for $\epsilon = 0.1$, $m = 0.5$, $J^* = 2000$ ($l = 0.5$ (——), 1.0 (– – –), 2.0 (·····)) and comparison with CBJ ($l = 0.5$ (+), 1.0 (△), 2.0 (○).

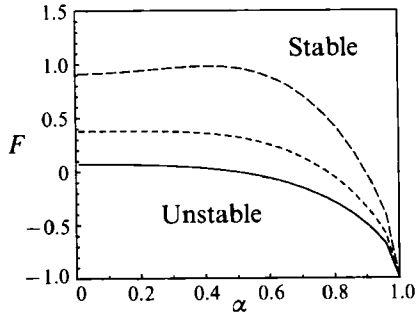

FIGURE 6. The m-dependence of the forced-flow neutral curves [F *vs.* α] for $\epsilon = 0.1$, $l = 1$, $\mathbb{R}_g = 10$, $J^* = 2000$ and $m < 1$ ($m = 0.3$ (——), 0.5 (---), 0.7 (---)).

Figure 5 shows a neutral curve F *vs.* α for a forced flow for various values of the density ratio l with the other parameters as in CBJ. Again the agreement is excellent and confirms CBJ's results that for forced flow heavy lubricants are stabilizing for downflow ($F > -1$) and light ones for upflow ($F < -1$). It is also interesting to note that when $l = 1$, the neutral curves are symmetric about $F = -1$. This is also clear from the equations. Since the term $F+1$ only enters the stability problem through the base flow and since for $l = 1$ a change in sign of $F+1$ just changes the direction of the base flow, such a change cannot affect the stability.

The final forced-flow neutral curve (figure 6) for $m < 1$, not given by CBJ, examines the effect of the viscosity ratio m. For downflow there exist a critical pressure gradient above which the system is stable and the pressure gradient needed for stability becomes smaller as the viscosity ratio gets smaller (see figure 6). The upflow region of this graph is not shown on this figure because for $l = 1$ the upflow curves are a mirror image of the downflow curves. As m increases the unstable lobe increases into a range of F in which the theory is no longer valid.

5.1.2. *The case of the more viscous annulus* ($m > 1$)

Since our concern is CAF stability in the context of liquid–liquid displacements of oil by water, the $m > 1$ situation is pertinent. Since F, unlike $\mathbb{R}_g$, is proportional to the experimentally manipulated pressure gradient, we present only the (F *vs.* α)-type neutral curve. For $m > 1$ (figure 7) viscosity stratification is destabilizing and thus

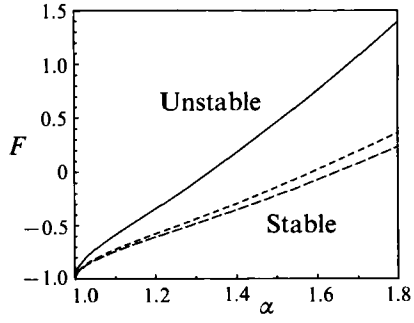

FIGURE 7. The m-dependence of the forced-flow neutral curves [F *vs.* α] for $\epsilon = 0.1$, $l = 1$, $\mathbb{R}_g^2 = 150$, $J^* = 2000$ and $m > 1$ ($m = 2$ (——), 10 (---), 100 (– – –)).

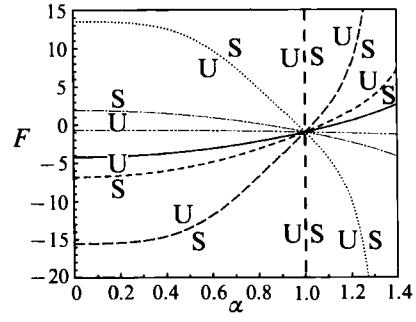

FIGURE 8. The l-dependence of the forced-flow neutral curves [F *vs.* α] in the absence of viscosity stratification ($m = 1$) for $\epsilon = 0.1$, $J^* = 10$, $\mathbb{R}_g = 10$ ($l = 0.1$ (——), 0.5 (---), 0.8 (– – –), 1.0 (– –), 1.2 (·····), 2.0 (—·—), 10.0 (—· · —)).

the band of unstable waves contains at least the band $0 < \alpha < 1$. In fact, this band grows as F or, in fact, as $\mathbb{R}_g$ (not shown) increases. Note again that for the $l = 1$ case, the upflow curve is just the reflection of the given (downflow) curve about $F = -1$. Hu & Joseph (1989) reported similar neutral curves [($\mathbb{R}$ *vs.* α)] for fixed $m > 1$, but larger values of J.

5.1.3. *The case of equal viscosities and unequal densities* ($m = 1$, $l \neq 1$)

As mentioned in §4, in the absence of viscosity stratification ($m = 1$) the density difference itself can compete with capillarity for moderate surface tension ($J = O(1)$). This is shown in figure 8 where we give neutral curves for different values of the density ratio l for $m = 1$, $J^* = 10$, $\mathbb{R}_g^2 = 10$, and $\epsilon = 0.1$. Obviously, the neutral curve at $\alpha = 1$ represents pure capillarity, the only surviving effect when $l = 1$. From this figure one sees that density stratification plays the same qualitative role as in the case $m < 1$, where it had only an order-ϵ effect on the stability. That is, heavy lubricants are stabilizing for downflow and destabilizing for upflow, while for light lubricants the opposite is true. The only difference is that in the absence of viscosity stratification, the density difference becomes a leading-order effect which can stabilize the capillary instability for sufficiently large pressure gradients that are downwards for heavy lubricants and upwards for light ones. Note that the figure displays a certain symmetry: when l is replaced by $2-l$ (for $2 \geqslant l \geqslant 0$) and F by $(-2-F)$, the curve remains unchanged. This, again, follows because the base flow simply changes direction upon these replacements.

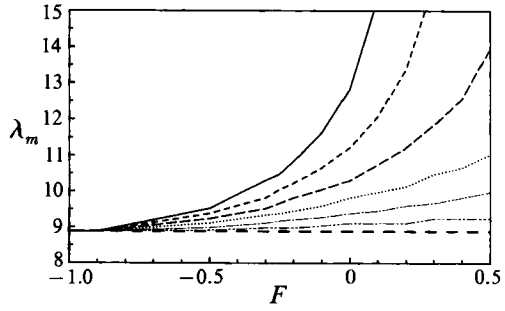

FIGURE 9. The m-dependence of the wavelength of maximum instability curves [λ_m *vs.* F] for $m \leqslant 1$, $\epsilon = 0.1$, $J^* = 2000$, $\mathbb{R}_g = 10$, $l = 1$ ($m = 0.4$ (——), 0.5 (- - -), 0.6 (— — —), 0.7 (·····), 0.8 (— · —), 0.9 (— · · —), 1.0 (– –)).

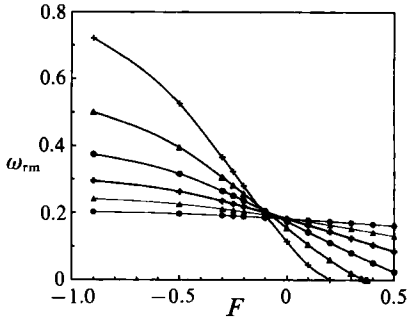

FIGURE 10. The m-dependence of the maximum growth rate curves [ω_{rm} *vs.* F] for $m < 1$, $\epsilon = 0.1$, $J^* = 2000$, $\mathbb{R}_g = 10$, $l = 1$ ($m = 0.4$ (+), 0.5 (△), 0.6 (○), 0.7 (+), 0.8 (▲), 0.9 (●)).

5.2. *Growth rates*

This brings us to a discussion of growth rates. We begin with the large-surface-tension, less viscous annulus situation, where we choose F to lie within the unstable lobe at the lower left of the canonical neutral curve. In figure 9 we show the wavelength of maximum instability from the linear analysis. For $m = 1$, there is no viscous stratification, and the wavelength of maximum instability is just the value determined by pure capillarity, which is independent of F. On the other hand, as m decreases from one, the film becomes less viscous and the effect of viscous stratification grows. The neutral curves exhibit this in that the intersection point of the neutral branch defining the surface-tension-derived unstable lobe with the F-axis decreases to -1. Similarly, since the maximally unstable wave is closely related to the critical wave, the curves in figure 9 (also symmetric about $F-1 = 0$) diverge at values of F that also recede towards $F = -1$ as m decreases from one.

The corresponding maximum growth rates (cf. figure 10) display competing effects. First, as the film becomes less viscous (i.e. m decreases from one), the system stabilizes, i.e. the maximum growth rate goes to zero, at lower values of F. Second, however, for values of F sufficiently far into the unstable region, the less viscous the film is, the less viscous resistance can inhibit the growth of unstable waves; thus small-m systems will grow faster than those with larger m values. This accounts for the cross-shape in figure 10.

Finally, we turn to the $m > 1$ and large-J case where, as already discussed, viscous stratification acts to destabilize the system (for small ϵ). The first trend that is clear

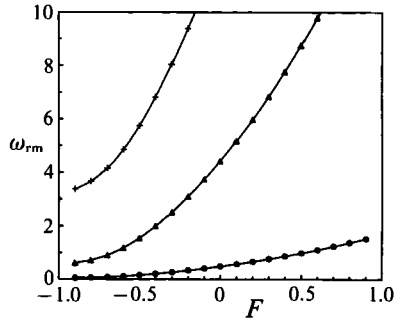

FIGURE 11. The m-dependence of the maximum growth rate curves [ω_{rm} *vs.* F] for $m > 1$, $\epsilon = 0.05$, $J^* = 2500$, $\mathbb{R}_g^2 = 150$, $l = 1$ ($m = 2$ (+), 10 (△), 100 (○)).

in figure 11 is that as F increases and the unstable band of waves broadens, the corresponding maximum growth rates also increase. The second trend is that as the film becomes more viscous, the maximum growth rates decrease; this is just the same effect that explained the left side of figure 10.

6. Stability of wetting layers in low-capillary-number slug flows

6.1. *An asymptotic theory in terms of Bretherton's scales*

When an aqueous phase displaces oil in a rock pore, slug flow regimes can arise in which the non-wetting phase takes the form of a train of long slugs moving over, and separated by, the wetting liquid. These flows are usually at very low capillary and slug-phase Reynolds numbers, where, in the notation of this paper, $\mathbb{C} = \mu_2 U/\sigma$ and $\mathbb{R} = \rho_1 V R_1/\mu_1$ and U is the slug velocity which for thin annuli is just $\frac{1}{2}V$.

Bretherton (1961) studied the motion of a long gas slug moving through a Newtonian liquid filling a straight cylindrical tube at low capillary and Reynolds numbers. Bretherton divided the slug interface and surrounding fluid into five regions: (i) a centre region where the wetting layer achieves a constant thickness; (ii) two tip regions where capillary forces are important and the interfacial shapes are, to leading order, sections of spheres; and (iii) two transition regions which bridge the tips and the constant-wetting-layer regions and in which capillary and viscous forces are both important and the wetting-layer fluid mechanics is described by the lubrication equations. By matching solutions is each of these regions in powers of the capillary number to the one-third power, Bretherton established the following leading-order equation for ϵ as $\mathbb{C} \to 0$:

$$\epsilon = 1.337\mathbb{C}^{\frac{2}{3}} + O(\mathbb{C}^{\frac{4}{3}}). \tag{6.1}$$

Park & Homsy (1984) re-examined Bretherton's problem for the case of interest here of a liquid slug, and demonstrated that the above expression for ϵ remains valid as long as the viscosity ratio m is larger than $\mathbb{C}^{\frac{1}{3}}$.

We use Bretherton's result to develop a theory for the stability of the wetting layer around a long liquid slug at low capillary numbers. We neglect density differences and express the stability equations in terms of $\mathbb{R}$ rather than F and $\mathbb{R}_g$ by the identification

$$\mathbb{R} = \frac{(F+1)}{4}\frac{(a^2-1+m)}{m}\mathbb{R}_g^2.$$

The growth rate may be expressed as an asymptotic expansion in $\mathbb{C}^{\frac{1}{3}}$ by introducing Bretherton's expression for ϵ into (4.6) and by equating $J/(m\mathbb{R})$ to $1/(2\mathbb{C})$. The result to order $\mathbb{C}^{\frac{4}{3}}$ is

$$c_i = -(1.337)^2\mathbb{C}\left(\frac{1.337}{2}i\alpha\frac{\alpha^2-1}{3}+\frac{1}{\alpha m}\left(1-\frac{1}{m}\right)\mathrm{Im}\,N(\alpha)\,\mathbb{C}^{\frac{1}{3}}+O(\mathbb{C}^{\frac{2}{3}})\right), \tag{6.2}$$

where c is now non-dimensionalized by the centreline velocity as in Preziosi *et al.* (1989). In the expression (A 14) for λ used in defining $N(\alpha)$, (6.2) replaces $\frac{1}{4}(F+1)\,\mathbb{R}_g^2$ by $\mathbb{R}$. Recall that (4.6) is valid for $m > \epsilon$ or $m > \mathbb{C}^{\frac{2}{3}}$ and the Bretherton expression is valid for $m > \mathbb{C}^{\frac{1}{3}}$. Since the latter is the more restrictive on m for $\mathbb{C} \ll 1$, the above expansion in $\mathbb{C}$ is valid for $m > \mathbb{C}^{\frac{1}{3}}$. Even with this restriction, one can draw some very interesting asymptotic conclusions regarding the growth dynamics:

(i) When $m < 1$ (oil slugs in water) and $\mathbb{C}^{\frac{1}{3}}$ is in the range $m > \mathbb{C}^{\frac{1}{3}} > m^2$, the stability is dominated by the stabilization due to viscosity stratification.

(ii) When $m < 1$ (again oil slugs in water), and $\mathbb{C}^{\frac{1}{3}}$ is smaller than or of the same order as m^2, capillarity competes with and then dominates the stabilizing effect of viscosity stratification.

(iii) When $m > 1$ (water drops in oil), for all $\mathbb{C} < 1$, viscosity stratification is destabilizing, but capillarity dominates.

Equation (6.2) can be the basis for constructing stability plots in $(\mathbb{R}, \mathbb{C})$-space for fixed $m < 1$. By setting the imaginary part of c equal to zero, one obtains

$$0 = 1.337\frac{\alpha(\alpha^2-1)}{6}+\frac{1}{\alpha m}\left(1-\frac{1}{m}\right)\mathrm{Im}\,(N(\alpha))\,\mathbb{C}^{\frac{1}{3}}. \tag{6.3}$$

One can calculate neutral stability plots of $\mathbb{R}$ against α for fixed $\mathbb{C}^{\frac{1}{3}}$ and m that would be of the same form as the $\mathbb{R}_g$ *vs.* α plots of §5. We suspect that for a fixed, small value of ϵ (and hence of $\mathbb{C}$) and $m < 1$, there is a range of m larger than $\mathbb{C}^{\frac{1}{3}}$ yet small enough that the lower branch of the neutral curves (e.g. figures 4, 5 and 6) is monotonic. In such cases, $\mathbb{R}_c$, just the limit of (6.3) as $\alpha \to 0$ given by

$$\mathbb{R}_c = 1.337\frac{2m^2\mathbb{C}^{-\frac{1}{3}}}{(1-m)}, \tag{6.4}$$

is the beginning of the window of global stability. The above equation defines a lobe in the $(\mathbb{C}^{\frac{1}{3}}, \mathbb{R})$-plane with unstable values lying inside the lobe. In view of the approximations involved in deriving (6.4), m must be less than one and $\mathbb{C}^{\frac{1}{3}}$ must be smaller than m. Also note that these approximations require that $\mathbb{R}$ be of order 1 in ϵ or $\mathbb{C}^{\frac{2}{3}}$. From (6.4) it is clear that this will be the case as long as $\mathbb{C}^{\frac{1}{3}}$ is larger than m^2; so (6.4) is valid for $m < 1$ and for capillary numbers in the interval $m > \mathbb{C}^{\frac{1}{3}} > m^2$.

One can use (6.4) to determine critical velocities above which oil slugs travel over linearly stable, thin water wetting layers. For such stable cases $\mathbb{R} > \mathbb{R}_c$ and therefore (6.4) leads to

$$U > [(1.337/(\rho_1 R_1 \mu_1))^3 \mu_2^5 \sigma]^{\frac{1}{4}}. \tag{6.5}$$

As a typical example, consider oil slugs of unit specific gravity and $\mu_1 = 10$ cP, travelling over a water film ($\mu_2 = 1$ cP) with an interfacial tension of 10 dynes/cm in a 250 μm diameter pore. The slug–film interface is linearly stable for $U > 0.6$ cm/s. However, inasmuch as the Bretherton theory breaks down for $\mathbb{C}^{\frac{1}{3}} > m$, this prediction formally holds only to $U \approx 1$ cm/s for the numbers given. Naturally, one would hope that the situation would not change qualitatively on exceeding the Bretherton restriction.

6.2. *The unstable case*; *Aul & Olbricht's experiments* ($m > 1$)

Aul & Olbricht (1990) performed experiments in which water displaced a much more viscous, immiscible fluid (glycol) of very similar density at low capillary numbers in a glass capillary with an inner diameter of 54 μm. They studied the stability of the wetting layers by video microscopy and observed undisturbed film thicknesses of 1–2 μm, or $\epsilon \sim 0.04$–0.07. Their experiments always yielded unstable wetting layers in the sense that interfacial disturbances grew and eventually pinched off the core. Aul & Olbricht observed the wavelength λ_m and wave speed c_r of the maximally growing unstable waves in these experiments. To compare theory with experiment, they neglected the effect of flow and calculated the value for λ_m arising purely from capillarity (which, as we shall see below, is exactly the leading-order term that results from our analysis). In addition, based on the assumption that the wave simply convects with the base velocity, they calculated a theoretical value for the wave speed. Their theoretical value for λ_m agrees quite well with the experimental value, although that for c_r does not.

Since Aul & Olbricht's experiments do indeed contain thin films, our theory should be able to address the validity of their neglecting of flow in the prediction of λ_c and of using only the convecting base-flow interfacial velocity for c_r. The parameters of the experiments are $\mathbb{R} = 0.0173$–0.0403; $J \sim 90$ and $m = 19, 80, 173$, where we have converted Aul & Olbricht's Reynolds numbers to our definition, as do Hu & Joseph (1989). We take $\mathbb{R} = \mathbb{R}_0 \epsilon$, $J = J_0/\epsilon$ and $m = m_0$ with m_0, J_0, $\mathbb{R}_0$ of order one. Using these values in our asymptotic analysis gives the leading orders of the real and imaginary parts of c non-dimensionalized with the centreline velocity as in (6.2) as

$$c_i = -\epsilon^2[J_0/(3m_0\mathbb{R}_0)]\,\alpha(\alpha^2-1) + O(\epsilon^3), \tag{6.6}$$

$$c_r - w^0(1) = c_r - (2\epsilon^2/m_0) + O(\epsilon^3) = -\frac{\epsilon^3}{m_0}\frac{\mathrm{Re}\,[N(\alpha;\mathbb{R}=0)]}{\alpha} + O(\epsilon^4). \tag{6.7}$$

Note that the leading order of $c - w^0(1)$ is purely imaginary and is exactly the expression used by Aul & Olbricht. Thus the leading order of c_r is $O(\epsilon^2)$, and is in fact simply the leading order of the base flow interfacial velocity. Thus Aul & Olbricht were correct (to leading order) in their neglect of viscous stratification in calculating the wavelength of maximum growth, and that is why λ_m is independent of $\mathbb{R}$ in their experiments.

In fact, these values for λ_m, as well as those for the leading-order growth rate (obtained in the usual way from the expression for c_i and are thus also independent of $\mathbb{R}$ to leading order), agree very well with those listed in table 4 of Hu & Joseph, who also examined Aul & Olbricht's data, calculating their numbers from the full, numerical solution of the Orr–Sommerfeld equations. The agreement between our equation (6.7) and Hu & Joseph's predictions for the wave speed is also very good (to within 10%). As a result, we believe that use of our asymptotic theory can be an excellent, simple guide for determining which will be the dominant effects in experiments with thin, annular films.

To determine which mechanism (viscosity stratification or capillarity) mainly drives the instability observed by Aul & Olbricht, Hu & Joseph did an energy analysis. In view of our having an explicit, asymptotic expression for the growth rate c, it seems superfluous at this point to perform Hu & Joseph's energy analysis for systems with thin annular films.

7. Weakly nonlinear interfacial evolution

An important aspect of developing a linear theory in the thin-film-thickness asymptotic regime, is its capability of readily producing the dominant weakly nonlinear system out of a gradual linear instability by ordering the disturbance parameter δ in (2.6) and (2.7) with ϵ. (A much larger initial disturbance would make both linear and weakly nonlinear theories redundant.) Such analyses have been performed by Papageorgiou *et al.* (1990) for the present geometry and for $m < 1$, but without density differences between the phases; the same formal procedure can be applied here also and the interested reader is referred to Papageorgiou *et al.* for details.

The main outcome of the asymptotic analyses of Papageorgiou *et al.* is the derivation of nonlinear evolution equations for $\delta = O(\epsilon^2)$ by incorporation of weak nonlinearities (as in the Burgers equation, for example) along with the linear operator that derives from the linear stability theory. Thus, it is easy to see that the evolution equation corresponding to our dispersion relation (4.6) is given by

$$\eta_\tau - \frac{2}{m}\frac{F+1}{4}\eta\eta_z + \frac{J_0}{3m\mathbb{R}_g^2}(\eta_{zz}+\eta_{zzzz}) - \frac{(l-1)}{2m}\eta_z - \mathrm{i}\frac{(m-1)}{2\pi m^2}\frac{F+1}{4} \times \int_{-\infty}^{\infty} N(\alpha)\int_{-\infty}^{\infty}\eta(z',\tau)\,\mathrm{e}^{\mathrm{i}\alpha(z-z')}\,\mathrm{d}z'\,\mathrm{d}\alpha = 0, \quad (7.1)$$

where $\tau = \epsilon^2 t$ is a stretched time. Equation (7.1) above covers a wide range of physical situations and is the result of 'large' surface tension as explained earlier. In the regime where $J/\mathbb{R}_g^2$ is order one and $m = 1$, disturbances grow on a relatively longer timescale (of order $1/\epsilon^3$ in fact) by virtue of the relative magnitude of density-difference instabilities (note that to leading order, a dispersive effect appears which is removed by a suitable Galilean transformation). The spectrum for this case is given by (4.6) and (4.7) and the evolution equation is

$$\eta_\tau - 2\frac{F+1}{4}\eta\eta_z + \frac{J}{3\mathbb{R}_g^2}(\eta_{zz}+\eta_{zzzz}) + \frac{(l-1)}{6}\eta_z + \mathrm{i}\frac{(l-1)}{4\pi} \times \int_{-\infty}^{\infty} N(\alpha)\int_{-\infty}^{\infty}\eta(z',\tau)\,\mathrm{e}^{\mathrm{i}\alpha(z-z')}\,\mathrm{d}z'\,\mathrm{d}\alpha = 0. \quad (7.2)$$

Most of the qualitative features of both evolution equations (7.1) and (7.2) have been explained by the numerical experiments of Papageorgiou *et al.* For instance, these experiments indicate that in the presence of capillarity the large-time nonlinear evolution of the system remains bounded and can, in many cases depending on relative magnitudes of flow parameters, produce intricate and varied behaviour ranging from trivial solutions to steady-state travelling waves to highly oscillatory chaotic behaviour. There is one regime, however, which is different and merits further discussion. This weakly nonlinear evolution arises from the problem of 'small' surface tension characterized by $J \sim 1$ and $\mathbb{R}_g^2 \sim 1$. The evolution equation is obtained by setting $J_0 = 0$ in (7.1) above and so the equation contains the viscosity stratification mechanism alone (similar comments and conclusions also apply for (7.2), again with $J = 0$). The flow becomes linearly unstable or stable depending on whether m is greater than or less than unity, respectively. The unstable case $m > 1$ has some novel nonlinear consequences and we describe a possible scenario next.

The large-wavenumber (short-wave) behaviour of the kernel $N(\alpha)$ is of particular importance. The asymptotic behaviour is $N(\alpha) \to \alpha|\alpha|$ as $\alpha \to \pm\infty$. So short waves, in the case $m > 1$ at least, grow the fastest and there does not exist a regularizing cutoff. The problem is then expected to break down within a finite time (note that special initial conditions need to be used – see comments and analysis in Papageorgiou & Smith 1988), the dominant structure being a shock formation in the interfacial shape. This shortening of axial lengthscales will invalidate our original assumptions of $O(1)$ wavelengths and bringing a new shorter lengthscale, governed by the structure of the finite-time singularity. New physics enters through the upgraded role of the surface-tension terms which are now in balance with viscous stratification due to the shorter scales involved. Overall then, the shock is expected to be smoothed out by the new physics that comes into play, and the final waveform should look like a saw-tooth wave. We note that this is merely a suggestion as to the final behaviour of the system when $J = O(1)$ and $\mathbb{R}_g^2 = O(1)$.

8. Summary and conclusions

We have developed an *analytic* asymptotic theory for the linear stability of a vertical, perfectly concentric, core–annular axial flow in the limit in which the annular gap $(R_2 - R_1)$ is much thinner than the core radius R_1, i.e.

$$\epsilon = (R_2 - R_1)/R_1 \ll 1.$$

Our theory includes the stability-determining factors: viscosity and density stratification through the ratios of the film to core viscosity $m(=\mu_2/\mu_1)$ and density $l(=\rho_2/\rho_1)$; interfacial tension σ through $J(=R_1\sigma\rho_1/\mu_1^2)$; and gravity and pressure-driven forcing through, respectively, a Reynolds number $\mathbb{R}_g^2(=\rho_1^2 g R_1^3/\mu_1^2)$ and the ratio $F(=(-\mathrm{d}P/\mathrm{d}z)/(\rho_1 g))$. A new, analytical, asymptotic expansion in ϵ of the complex wave speed complete to order ϵ^3 results for the general case of m and l of order one, F and $\mathbb{R}_g^2$ of order one or less and J of arbitrary order. It allows a clear, asymptotic ordering of the destabilizing forces in terms of ϵ. In particular, capillarity first enters the growth rate at order $J\epsilon^3/m\mathbb{R}_g^2$, while, for $\mathbb{R}_g^2 = O(1)$, viscosity stratification contributes at order $(m-1)\epsilon^2/m^2$ and density at orders $(l-1)\epsilon^3/m$ and $(l-1)\epsilon^3/m^2$. In addition, viscosity and density are strongly dispersive: they both generate a leading-order ($O(\epsilon^2)$) wave speed in the frame travelling with the interface velocity. Certain conclusions, valid as $\epsilon \to 0$, follow immediately. (i) The film's inertia is not important and is a second-order effect. (ii) For moderate surface tension, viscosity stratification dominates and the system is stable when the less viscous fluid is in the film and unstable when the less viscous fluid is in the core. (iii) For strong surface tension, capillarity competes with viscosity stratification, and (iv) density stratification is purely dispersive to leading order; its stability contribution is a second-order effect. Finally, for films of sufficiently low viscosity, viscosity stratification and capillarity determine the growth rates of wetting layers in slug flows.

Our asymptotic theory depicts the linear stability for thin films very well. Comparison with results of Joseph and co-workers who numerically solved the Orr–Sommerfeld equations shows excellent agreement (cf. figures 3, 4 and 5), for ϵ as large as 0.2.

The expansion also leads to new linear stability results for wetting layers in low-capillary-number $\mathbb{C}$ liquid–liquid displacements, where ϵ scales as $\mathbb{C}^{\frac{1}{3}}$. The resulting expression (in $\mathbb{C}^{\frac{1}{3}}$) for the wave speed includes both capillarity and viscous

stratification and provides a guide for determining which effects dominate wetting-layer stability in a particular flow regime. It correctly predicts the liquid–liquid displacement experiments of Aul & Olbricht (1990), and verifies their assumption that capillarity dominates their flow regime.

Finally we follow instabilities to the weakly nonlinear regime by deriving interfacial amplitude equations. These non-local Kuramoto–Sivashinsky-like equations contain a nonlinear term arising from the shear nature of the base flow, which shocks the interface into shorter scales, and an interfacial tension term which acts to stabilize precisely those scales. In lubricated pipelining, $m < 1$ and capillarity effects are less important ($J < O(1)$); the interplay with capillarity at a later stage may lead to a sharp, saw-toothed interfacial shape.

Appendix

Substituting the expansion (4.3)–(4.5) into the governing equations and boundary conditions of a system with new coordinates travelling with the base-state velocity at the interface $[w_1^{(0)}(1)]$ of the base state, we get, to leading order in ϵ

$$\mathrm{D}(\mathrm{D}\psi_1^{(0)}) = \mathrm{i}\alpha\mathbb{R}_g^2\frac{F+1}{4}(1-r^2)\,\mathrm{D}\psi_1^{(0)}, \tag{A 1}$$

$$\frac{\mathrm{d}^4\psi_2^{(2)}}{\mathrm{d}y^4} = 0, \tag{A 2}$$

$$\psi_1^{(0)} = 0 \quad \text{at} \quad r = y = 1, \tag{A 3}$$

$$\frac{\mathrm{d}\psi_1^{(0)}}{\mathrm{d}r} - \left(1-\frac{1}{m}\right)\frac{F+1}{2}\frac{\psi_2^{(2)}}{\bar{c}^{(2)}} = 0 \quad \text{at} \quad r = y = 1, \tag{A 4}$$

$$\mathrm{D}\psi_1^{(0)} - m\frac{\mathrm{d}^2\psi_2^{(2)}}{\mathrm{d}y^2} + 2\alpha^2(1-m)\,\psi_1^{(0)} + (l-1)\frac{\psi_2^{(2)}}{\bar{c}^{(2)}} = 0 \quad \text{at} \quad r = y = 1, \tag{A 5}$$

and

$$-\mathrm{i}\alpha m\frac{\mathrm{d}^3\psi_2^{(2)}}{\mathrm{d}y^3} - \frac{J_0}{\mathbb{R}_g^2}(\alpha^4-\alpha^2)\frac{\psi_2^{(2)}}{\bar{c}^{(2)}} = 0 \quad \text{at} \quad r = y = 1, \tag{A 6}$$

where $J_0 = J\epsilon$ and $\bar{c} = c - w^0(1) = \bar{c}^{(2)}\epsilon^2 + \bar{c}^{(3)}\epsilon^3 + O(\epsilon^4)$.

The next order in ϵ gives

$$\mathrm{D}(\mathrm{D}\psi_1^{(1)}) = \mathrm{i}\alpha\mathbb{R}_g^2\frac{F+1}{4}(1-r^2)\,\mathrm{D}\psi_1^{(1)}, \tag{A 7}$$

$$\frac{\mathrm{d}^4\psi_2^{(3)}}{\mathrm{d}y^4} = -\frac{2}{r^3}\frac{\mathrm{d}^3\psi_2^{(2)}}{\mathrm{d}y^3}, \tag{A 8}$$

$$\psi_1^{(1)} = 0 \quad \text{at} \quad r = y = 1, \tag{A 9}$$

$$\frac{\mathrm{d}\psi_1^{(1)}}{\mathrm{d}r} - \left(1-\frac{1}{m}\right)\frac{F+1}{2}\frac{\psi_2^{(3)}}{\bar{c}^{(2)}} = -\frac{\mathrm{d}\psi_2^{(2)}}{\mathrm{d}y} - \left(1-\frac{1}{m}\right)\frac{F+1}{2}\frac{\psi_2^{(2)}\bar{c}^{(3)}}{(\bar{c}^{(2)})^2} \quad \text{at} \quad r = y = 1, \tag{A 10}$$

$$\mathrm{D}\psi_1^{(1)} - m\frac{\mathrm{d}^2\psi_2^{(3)}}{\mathrm{d}y^2} + 2\alpha^2(1-m)\,\psi_1^{(1)} + (l-1)\frac{\psi_2^{(3)}}{\bar{c}^{(2)}} = m\frac{\mathrm{d}\psi_2^{(2)}}{\mathrm{d}y} + (l-1)\frac{\psi_2^{(2)}\bar{c}^{(3)}}{(\bar{c}^{(2)})^2} \quad \text{at} \quad r = y = 1, \tag{A 11}$$

and

$$-\mathrm{i}\alpha m\frac{\mathrm{d}^3\psi_2^{(3)}}{\mathrm{d}y^3}-\frac{J_0}{\mathbb{R}_g^2}(\alpha^4-\alpha^2)\frac{\psi_2^{(3)}}{\bar{c}^{(2)}}=\mathrm{i}\alpha m\frac{\mathrm{d}^2\psi_2^{(2)}}{\mathrm{d}y^2}-\frac{J_0}{\mathbb{R}_g^2}(\alpha^4-\alpha^2)\frac{\psi_2^{(2)}\bar{c}^{(3)}}{(\bar{c}^{(2)})^2}$$

$$+\mathrm{i}\alpha\frac{\mathrm{d}}{\mathrm{d}r}(\mathrm{D}\psi_1^{(0)}-2\alpha^2\psi_1^{(0)})\quad\text{at}\quad r=y=1. \tag{A 12}$$

Following Papageorgiou *et al.* (1990) and Pekeris (1948) one can solve the leading-order core problem in terms of Kummer or confluent hypogeometric functions $M(\Lambda,2,\lambda r^2)$ (see Abramowitz & Stegun 1972), where

$$\Lambda=1+\alpha^2/8\lambda-\lambda/2, \tag{A 13}$$

and

$$\lambda=\tfrac{1}{4}[\alpha\mathbb{R}_g^2(F+1)]^{\frac{1}{2}}\mathrm{e}^{-\mathrm{i}\pi/4}. \tag{A 14}$$

The solution for the stream function in the core becomes

$$(1/r)\psi_1^{(0)}=A_1(\alpha)I_1(\alpha r)+B_1(\alpha)N_1(\alpha r), \tag{A 15}$$

where

$$N_1(\alpha r)=\int_0^r[I_1(\alpha r)K_1(\alpha t)-I_1(\alpha t)K_1(\alpha r)]\,t^2\,\mathrm{e}^{-\lambda t^2}M(\Lambda,2,2\lambda t^2)\,\mathrm{d}t. \tag{A 16}$$

The solution in the annulus that satisfies no slip at the wall ($y=0$) is

$$\psi_2^{(2)}=A_2y^3+B_2y^2. \tag{A 17}$$

Applying the leading-order interfacial boundary conditions (A 3)–(A 6) we get a (4×4) system of equations of the form

$$\boldsymbol{A}\cdot\boldsymbol{x}=\boldsymbol{0}. \tag{A 18}$$

The matrix

$$\boldsymbol{A}=\begin{bmatrix} I_1(\alpha) & N_1(\alpha) & 0 & 0\\ \alpha I_0(\alpha) & \alpha N_2(\alpha) & -\left(1-\dfrac{1}{m}\right)\dfrac{F+1}{2\bar{c}^{(2)}} & -\left(1-\dfrac{1}{m}\right)\dfrac{F+1}{2\bar{c}^{(2)}}\\ 2\alpha^2(1-m)I_1(\alpha) & \mathrm{e}^{-\lambda}M(\Lambda,2,2\lambda)+2\alpha^2(1-m)N_1(\alpha) & -6m+\dfrac{(l-1)}{\bar{c}^{(2)}} & -2m+\dfrac{(l-1)}{\bar{c}^{(2)}}\\ 0 & 0 & 6m\mathrm{i}\alpha+\dfrac{J_0}{\mathbb{R}_g^2}\dfrac{\alpha^2(\alpha^2-1)}{\bar{c}^{(2)}} & \dfrac{J_0}{\mathbb{R}_g^2}\dfrac{\alpha^2(\alpha^2-1)}{\bar{c}^{(2)}} \end{bmatrix}$$

in (A 18) contains the coefficients of the constants of integration in these linearized boundary conditions. The constants appearing in $\boldsymbol{A}$ are

$$N_1(\alpha)=\int_0^1[I_1(\alpha)K_1(\alpha t)-I_1(\alpha t)K_1(\alpha)]\,t^2\,\mathrm{e}^{-\lambda t^2}M(\Lambda,2,2\lambda t^2)\,\mathrm{d}t, \tag{A 19}$$

$$N_2(\alpha)=\int_0^1[I_0(\alpha)K_1(\alpha t)+I_1(\alpha t)K_0(\alpha)]\,t^2\,\mathrm{e}^{-\lambda t^2}M(\Lambda,2,2\lambda t^2)\,\mathrm{d}t. \tag{A 20}$$

Finally $\boldsymbol{x}$ is the vector of the constants of integration

$$\boldsymbol{x}=[A_1,B_1,A_2,B_2]^{\mathrm{t}}. \tag{A 21}$$

The amplitude equation follows by solving the equation $\det(\boldsymbol{A})=0$ in terms of the wave speed $\bar{c}^{(2)}$ (to order ϵ^2); the result is (4.6), i.e.

$$\bar{c}^{(2)} = -\frac{J_0}{3m\mathbb{R}_g^2}\alpha(\alpha^2-1)\,\mathrm{i}+\frac{1}{m}\frac{F+1}{4}\left[-\frac{N(\alpha)}{\alpha}\left(1-\frac{1}{m}\right)\right]+\frac{(l-1)}{2m},$$

where

$$N(\alpha) = \frac{I_1(\alpha)\,\mathrm{e}^{-\lambda}M(\Lambda,2,2\lambda)}{N_1(\alpha)I_0(\alpha)-N_2(\alpha)I_1(\alpha)}, \tag{A 22}$$

which is, in general, complex.

The general solution to the governing equation in the core remains the same to the next order in ϵ but the solution to the governing equation in the film that satisfies no slip on the wall becomes

$$\psi_2^{(3)} = a_2 y^3 + b_2 y^2 - \tfrac{1}{2}A_2 y^4. \tag{A 23}$$

Applying the second-order boundary conditions (A 9) to (A 12) we get a system of equations of the form

$$\boldsymbol{A}\cdot\boldsymbol{x} = \boldsymbol{b}, \tag{A 24}$$

where $\boldsymbol{A}$ is the same as in (A 18) and $\boldsymbol{x}$ is the new vector of the constants of integration to this order in ϵ. Finally, $\boldsymbol{b}$ is a vector containing the inhomogeneities to this order in ϵ given by

$$\boldsymbol{b} = \begin{bmatrix} 0 \\ -\left(\dfrac{(1-1/m)\,(F+1)}{2\bar{c}^{(2)}}\left(\dfrac{1}{2}+\dfrac{\bar{c}^{(3)}}{\bar{c}^{(2)}}\right)+3\right)A_2-\left(\dfrac{(1-1/m)\,(F+1)}{2(\bar{c}^{(2)})^2}+2\right)B_2 \\ \left(\dfrac{(l-1)}{\bar{c}^{(2)}}\left(\dfrac{1}{2}+\dfrac{\bar{c}^{(3)}}{\bar{c}^{(2)}}\right)-3m\right)A_2+\left(\dfrac{(l-1)\,\bar{c}^{(3)}}{(\bar{c}^{2})^2}+2m\right)B_2 \\ \left(\dfrac{J_0\alpha^2(\alpha^2-1)}{\mathbb{R}_g^2\bar{c}^{(2)}}\left(\dfrac{1}{2}-\dfrac{\bar{c}^{(3)}}{\bar{c}^{(2)}}\right)+6mi\alpha\right)A_2-\left(\dfrac{J_0\alpha^2(\alpha^2-1)\,\bar{c}^{(3)}}{\mathbb{R}_g^2(\bar{c}^{(2)})^2}-2mi\alpha\right)B_2 \\ -2\mathrm{i}\alpha^4 I_0(\alpha)A_1+\left(-2\mathrm{i}\alpha^4 N_2(\alpha)+\mathrm{i}\alpha\dfrac{\mathrm{d}}{\mathrm{d}r}(r^2\,\mathrm{e}^{-\lambda r^2}M(\Lambda,2,2\lambda r^2))\right)B_1 \end{bmatrix}.$$

Using the solvability (adjoint) method we solve (A 24) for the wave speed $\bar{c}^{(3)}$ (to order ϵ^3); the result is (4.7), i.e.

$$\bar{c}^{(3)} = -\frac{J_0}{\mathbb{R}_g^2}\frac{N(\alpha)}{4m^2}(\alpha^2-1)\,\mathrm{i}+\left[-\frac{1}{6m}+\frac{N(\alpha)}{2\alpha m^2}\right](l-1)$$
$$-\left[\frac{2\alpha^2}{3m}+\frac{2T(\alpha)-N(\alpha)}{6\alpha m}+\frac{N^2(\alpha)}{2\alpha^2m^2}\right]\left(1-\frac{1}{m}\right)\frac{F+1}{2},$$

where

$$T(\alpha) = \frac{I_1(\alpha)\,\mathrm{e}^{-\lambda}M(\Lambda+1,3,2\lambda)}{N_1(\alpha)I_0(\alpha)-N_2(\alpha)I_1(\alpha)}, \tag{A 25}$$

which is also, in general, complex.

REFERENCES

Abramowitz, M. & Stegun, I. A. 1972 *Handbook of Mathematical Functions*. Dover.

Aul, R. W. & Olbricht, W. L. 1990 Stability of a thin annular film in pressure-driven, low-Reynolds-number flow through a capillary. *J. Fluid Mech.* **215**, 585–599.

Bai, R., Chen, K. & Joseph, D. D. 1990 Lubricated pipelining: stability of core–annular flow. Part 5. Experiments and comparison with theory. *J. Fluid Mech.* **240**, 97–132.

BRETHERTON, F. P. 1961 The motion of long bubbles in tubes. *J. Fluid Mech.* **10**, 166–188.

CHANDRASEKHAR, S. 1968 *Hydrodynamic and Hydromagnetic Stability*. Oxford University Press.

CHEN, K. P. 1992 Short wave instabilities of core annular flow. *Phys. Fluids* A **4**, 186–188.

CHEN, K., BAI, R. & JOSEPH, D. D. 1990 Lubricated pipelining. Part 3. Stability of core–annular flow in vertical pipes. *J. Fluid Mech.* **214**, 251–286 (referred to herein as CBJ).

CHEN, K. & JOSEPH, D. D. 1991 Long waves and lubrication theories for core annular flow. *Phys. Fluids* A **3**, 2672–2679.

GAUGLITZ, P. A. & RADKE, C. J. 1990 The dynamics of liquid film breakup in constricted cylindrical capillaries. *J. Colloid Interface Sci.* **134**, 14–40.

GOREN, S. L. 1962 The instability of an annular thread of fluid. *J. Fluid Mech.* **27**, 309–319.

HICKOX, C. E. 1971 Instability due to viscosity and density stratification in axisymmetric pipe flow., *Phys. Fluids* **14**, 251–262.

HU, H. H. & JOSEPH, D. D. 1989 Lubricated pipelines: stability of core–annular flow. Part 2. *J. Fluid Mech.* **205**, 359–396.

HU, H., LUNDGREN, T. & JOSEPH, D. D. 1990 Stability of core-annular flow with a small viscosity ratio. *Phys. Fluids* A **2**, 1945–1954.

JOSEPH, D. D., RENARDY, Y. & RENARDY, M. 1984 Instability of the flow of immiscible liquids with different viscosities in a pipe. *J. Fluid Mech.* **141**, 309–317.

NEWHOUSE, L. A. & POZRIKIDIS, C. 1992 The capillary instability of annular layers and liquid threads. *J. Fluid Mech.* **242**, 193–209.

PAPAGEORGIOU, D. T., MALDARELLI, C. & RUMSCHITZKI, D. S. 1990 Nonlinear interfacial stability of core–annular film flows. *Phys. Fluids* A **2**, 340–352.

PAPAGEORGIOU, D. T. & SMITH, F. T. 1988 Nonlinear instability of the wake behind a flat plate placed parallel to a uniform stream. *Proc. R. Soc. Lond.* A **419**, 1–28.

PARK, C. W. & HOMSY, G. M. 1984 Two-phase displacement in Hele–Shaw cells: theory. *J. Fluid Mech.* **139**, 291–308.

PEKERIS, C. L. 1948 Stability of the laminar flow through a straight pipe of circular cross-section to infinitesimal disturbances which are symmetrical about the axis of the pipe. *Proc. Natl Acad. Sci. USA* **34**, 285–295.

PREZIOSI, K., CHEN, K. & JOSEPH, D. D. 1989 Lubricated pipelines: Stability of core–annular flow. *J. Fluid Mech.* **201**, 323–356.

RATOLOWSKI, J. & CHANGE, H. C. 1989 In Snap-off at strong constrictions: effect of pore geometry. In *Surface-Based Mobility Control: Progress in Miscible Flood Enhanced Oil Recovery* (ed. D. H. Smith). ACS Symposium Series, vol. 33, pp. 282–314. Hemisphere.

SMITH, M. K. 1989 The axisymmetric long wave instability of a concentric two-phase pipe flow. *Phys. Fluids* A **1**, 494–506.

TOMOTIKA, S. 1935 On the instability of a cylindrical thread of a viscous liquid surrounded by another viscous liquid. *Proc. R. Soc. Lond.* A **150**, 322–337.

YIH, C. S. 1967 Instability due to viscosity stratification. *J. Fluid Mech.* **27**, 337–352.